Research Article | Vol. 27, No. 3 | 4 Feb 2019 | OPTICS EXPRESS 3190
Optics EXPRESS

An unstabilized femtosecond semiconductor laser for dual-comb spectroscopy of acetylene

JACOB NÜRNBERG,[1,3,*] CESARE G. E. ALFIERI,[1,3] ZAIJUN CHEN,[2] DOMINIK WALDBURGER,[1] NATHALIE PICQUÉ,[2] AND URSULA KELLER[1]

[1]*Department of Physics, Institute for Quantum Electronics, ETH Zürich, 8093 Zürich, Switzerland*
[2]*Max-Planck Institute of Quantum Optics, Hans-Kopfermann-Straße 1, 85748 Garching, Germany*
[3]*These authors contributed equally*
**njacob@phys.ethz.ch*

Abstract: Dual-comb systems based on two optical frequency combs of slightly different line spacing emerge as powerful tools in spectroscopy and interferometry. Semiconductor lasers have a high impact in continuous-wave tunable laser spectroscopy. Here we demonstrate the first dual-comb interferometer based on a single femtosecond semiconductor laser: a dual-comb modelocked optically pumped external-cavity surface-emitting laser (MIXSEL) ideally suited for a 1 to 10 GHz comb spacing. At a center wavelength of 1.03 µm (9709 cm^{-1}) we measured acetylene gas transmittance with a resolution of 2.7 GHz in 100 ms with residual errors of less than 3% using thousand comb lines without aliasing effects.

1. Introduction

An optical frequency comb (OFC) [1–3] consists of equidistant phase-coherent spectral lines, spaced by a frequency interval f_{rep} and shifted from the origin by an offset f_{CEO}. Such radio-frequency-referenced OFCs provide frequency rulers that enable accurate frequency, time and distance measurements [4]. Dual-comb spectroscopy (DCS) [5,6] measures the time-domain interference between two OFCs of slightly different line spacing $f_{rep,1}$ and $f_{rep,2} = f_{rep,1} + \Delta f_{rep}$ on a single photo-detector within short cycling times ($t_{min} = 1/\Delta f_{rep}$) and converts broadband optical spectra to the radio-frequency domain. With dual-comb spectrometers based on self-referenced modelocked lasers, self-calibrated spectra with an instrumental line-shape that may be neglected are obtained in the near- [7] and mid-IR [8] for arbitrarily long integration times. However, such systems rely on elaborate electronics and/or digital processing to maintain or reconstruct the coherence between the two combs. To overcome complexity, several solutions explored dual-comb systems with intrinsic long coherence, such as for example with ring cavity solid state laser [9], modelocked fiber laser [10,11], electro-optical modulator [12] or micro-resonator [13]. Electrically pumped semiconductor lasers such as quantum cascade lasers (QCLs) [14,15] and interband cascade lasers (ICLs) [16,17] have raised remarkable spectroscopic interest due to their direct emission in the mid-IR. Their line spacing (typically ≈10 GHz) on the other hand is usually too large for transitions of molecules in the gas phase and their span (typically <100 lines) is still rather narrow. Optically pumped semiconductor disk lasers (SDLs) [18,19] cover a spectral range from visible to mid-IR and only recently appeared as a promising technology for DCS [20]. First dual-comb operation has been obtained in hybrid SDL-fiber systems [21] and with a picosecond optically pumped modelocked integrated external-cavity surface-emitting laser (MIXSEL) [22].

Here, we show dual-comb spectroscopy on acetylene using a single-source dual-comb semiconductor laser without active stabilization or external amplification. A femtosecond MIXSEL emits two pulse trains with an adjustable comb-spacing difference at a wavelength of 1.03 µm (9709 cm^{-1}). We measure acetylene gas transmittance with a resolution of 2.7 GHz without aliasing effects in 100 ms with residual errors of less than 3%. Compared to

#349223 https://doi.org/10.1364/OE.27.003190
Journal © 2019 Received 29 Oct 2018; revised 28 Dec 2018; accepted 2 Jan 2019; published 30 Jan 2019

Optics EXPRESS

other semiconductor-based dual-comb sources [14,16], the dual-comb MIXSEL [23] with its 1-5 GHz comb spacing is ideally suited for spectroscopy applications.

The MIXSEL generates a modelocked pulse train from a linear straight cavity defined by the MIXSEL chip and the output coupler (OC) as the two end mirrors. The cavity length sets the pulse repetition rate and therefore the comb spacing, i.e. for example a 3 GHz OFC requires an optical cavity length of 5 cm. The MIXSEL combines the advantages of a passively modelocked laser oscillator providing a high pulse peak power and broad bandwidth with the compactness and wavelength versatility typical of semiconductor lasers. In dual-comb operation, the initially unpolarized beam is split towards the semiconductor MIXSEL chip with intracavity birefringent crystals (BCs) (Fig. 1(a)). Two OFCs are then generated in the same straight laser resonator and intrinsically achieve high mutual coherence. In contrast to other integrated semiconductor dual-comb systems, the MIXSEL provides excellent beam quality ($M^2 < 1.1$) and a high degree of flexibility in frequency mode spacing [24] (1-100 GHz), which can be controlled independently from the carrier-envelope offset. Furthermore, the difference in pulse repetition rate between the cross-polarized OFCs is finely adjustable via thickness and orientation of the BCs [23]. The first dual-comb MIXSEL spectroscopy proof-of-principle demonstration was based on long picosecond pulses with typically ≈0.4 nm (128 GHz) of full optical bandwidth [20], making them less attractive for spectroscopy applications. In this letter, we introduce a new generation of MIXSEL chips and demonstrate real-time DCS of acetylene with a free running femtosecond dual-comb MIXSEL emitting at 1030 nm.

2. Description of the laser

Extensive epitaxial and structural novelties are implemented to obtain sub-ps pulses and several nanometers of optical bandwidth in dual-comb operation. The epitaxial MIXSEL chip consists of a bottom GaAs/$Al_{0.98}Ga_{0.02}As_{0.98}P_{0.02}$ distributed Bragg reflector (DBR) with the high reflectivity bandwidth centered at 1030 nm. A single InGaAs QW absorber follows the DBR to enable passive modelocking. A second AlAs/$Al_{0.15}Ga_{0.85}As$ DBR reflects the residual pump light to prevent unwanted saturation of the saturable absorber. The strain compensated active region with 11 InGaAs QWs embedded in GaAs barriers acts as laser gain medium. Finally, a 3-pair dielectric top coating finalizes the structure and optimized the cavity roundtrip group delay dispersion. The layers are optimized to obtain a superior surface homogeneity and an efficient transversal 1D heat removal beneficial for dual-spot pumping and dual-comb operation [25]. Following our pulse shortening strategies [26], we carefully engineer the chip group delay dispersion through multipair numerically-optimized dielectric top coatings. Additionally, large bandgap AlAsP strain compensation materials are developed for better carrier confinement and low two-photon absorption losses in the region of the active quantum wells (QW). Finally, we decrease the growth temperature of the absorber QW for a shorter recovery time and a sharper temporal pulse shaping. This, together with a structurally broad and flat gain profile, allows for femtosecond pulse generation.

The full structure of the dual-comb modelocked integrated external-cavity surface-emitting laser (MIXSEL) is shown in Fig. 1(a). The laser cavity is build up from two basic elements: the MIXSEL chip and a curved output coupler with a 100-mm radius of curvature and a 0.1% output coupler. For dual-comb MIXSEL operation, the semiconductor chip is optically pumped with a single multimode pump diode (LIMO35-F100-DL808) at 808 nm whose beam is split with a 50:50 beam splitter (BS) to simultaneously pump two distinct spots on the semiconductor chip (Fig. 1(a)).

Two 0.5-mm thick wedged intracavity calcite ($CaCO_3$) birefringent crystals separate the initially unpolarized laser beam into two cross polarized pulse trains. By using two orthogonally oriented crystals, we nominally add the same optical path length to either polarization. Translating one of the wedged crystals further into the beam, allows to control the relative path lengths difference and thus the difference in repetition rate.

Optics EXPRESS

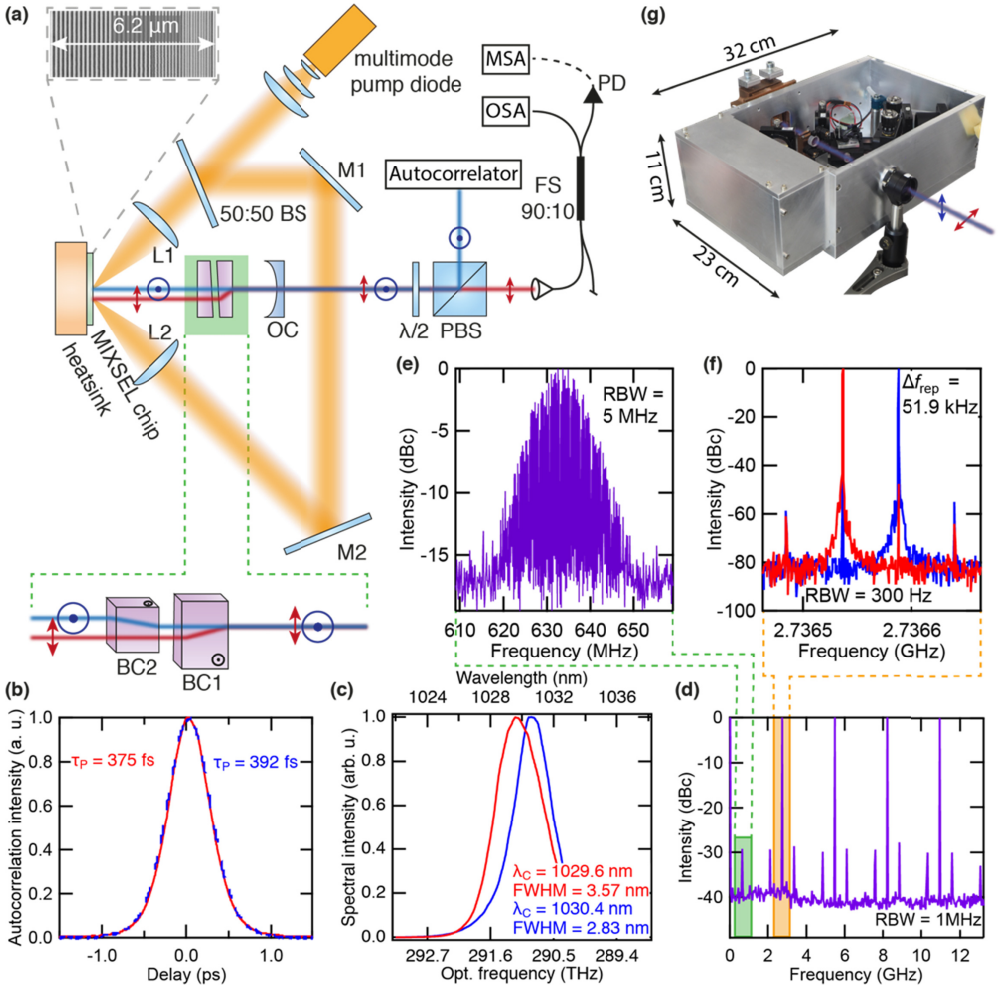

Fig. 1. Laser Setup and Characterization of Dual-Comb Modelocking. a) Dual-comb MIXSEL: The linear MIXSEL cavity is defined by the MIXSEL chip and the output coupler as the two end mirrors. The intracavity birefringent crystals (BCs) enable dual-comb operation. The semiconductor MIXSEL chip incorporates gain and saturable absorber quantum wells within a 6.2 µm thick structure with > 120 epitaxial layers (zoom: scanning electron microscope image). For dual-comb operation at small Δf_{rep}, two intracavity cross-oriented, wedged BCs divide the non-polarized cavity beam towards the MIXSEL side. The same diode simultaneously pumps two spots on the MIXSEL chip. The collinear cross-polarized output pulse trains can be combined or separated by turning a λ/2-waveplate followed by a PBS to reach the laser diagnostics. MSA: microwave spectrum analyzer, OSA: optical spectrum analyser, PD: photodetector, BS: beam splitter, PBS: polarising beam splitter, BC: birefringent crystal, OC: output coupler, L: lens, M: mirror, FS: fiber splitter. b) Autocorrelation traces. c) Optical spectra. d) Long-span microwave spectrum of the pulse trains projected on the same polarization, acquired with a resolution bandwidth (RBW) of 1 MHz. e) Zoom of the radio frequency comb generated by OFCs' beating. f) Peaks corresponding to the fundamental pulse repetition rates of the OFCs with a linewidth below the resolution bandwidth of 300 Hz. g) Photo and dimensions of the femtosecond dual-comb MIXSEL prototype.

3. Laser performance

Both OFC beams at the exit of the dual-comb MIXSEL are collinear and superimposed but orthogonally polarized. To separate both OFCs for diagnosis, the beam is directed through a λ/2-waveplate and a polarizing beam splitter (PBS). By rotation of the waveplate, each beam can by individually characterized. The laser performance is characterized as follows. First, the

Optics EXPRESS

pulse shape and duration is estimated from an intensity autocorrelation measurement (Femtochrome Research, FR-103HS). Second, the spectral characteristics of each comb are observed on an optical spectrum analyzer (OSA) (Hewlett-Packard, 70004A). Third, the laser is detected with a photodiode (PD) (NewFocus, Model: 1014) and a microwave spectrum analyzer (MSA) (Agilent E4405B) is employed to observe the repetition rates and its higher harmonics.

With the new chips, the pulse duration for the two OFCs is reduced from 18 ps [20] to sub 400 fs (Fig. 1(b)) and the usable optical bandwidth increases accordingly. The emission wavelength of the active QWs is tuned to match the position of the ro-vibrational lines in the region of the $3\nu_3$ band of acetylene. Due to surface inhomogeneity, the average output powers of the two modelocked beams differ slightly (28 and 24 mW) and the optical spectra are not perfectly coinciding. Nevertheless, the spectral coverage of the fs dual-comb MIXSEL spans more than 10 nm (> 2.5 THz) around 1030 nm (291 THz / 9709 cm^{-1}) (Fig. 1(c)). Additionally, both OFCs are combined in the same polarization by rotating the waveplate to a $\pi/8$. They interfere on the photodetector and the MSA detects both the radiofrequency beat signal and the repetition rates (Figs. 1(d)-1(f)). To sample absorption profiles with sufficient resolution and in a rapid manner, we set the MIXSEL cavity length to ≈55 mm for a mode spacing of 2.73 GHz.

4. Spectral aliasing

The beating of the two optical frequency combs generates down-converted microwave frequency combs symmetrically spaced around the pulse repetition rate and its harmonics. To avoid aliasing effects between these combs [27], the resolvable width of the comb Δf_{rf} in the radio-frequency domain must fulfill:

$$\Delta f_{rf} < \frac{f_{rep}}{2} \tag{1}$$

where f_{rep} is the fundamental pulse repetition rate considered as $(f_1 + f_2)/2$, where f_1 and f_2 are the two pulse repetition rates of the dual comb system ($\Delta f_{rep} \ll f_{rep}$). The resolvable width of the comb Δf_{rf} in the radio-frequency domain is given by:

$$\Delta f_{rf} = \Delta f_{opt} \frac{\Delta f_{rep}}{f_{rep}}. \tag{2}$$

Combining Eqs. (1) and Eq. (2), we obtain a condition on Δf_{rep}:

$$\Delta f_{rep} < \frac{f_{rep}^2}{2\Delta f_{opt}} \tag{3}$$

where Δf_{opt} is the resolvable optical laser bandwidth. In the dual-comb MIXSEL, Δf_{rep} derives from the different optical path length for the two cross-polarized beams in the birefringent crystals. In the case of two orthogonally oriented wedged crystals we can write:

$$\Delta f_{rep} = \frac{c}{2} \cdot \left(\frac{1}{L_0 + L_1 + \frac{L_2}{\cos\rho}} - \frac{1}{L_0 + \frac{L_1}{\cos\rho} + L_2 + \varepsilon} \right). \tag{4}$$

Here ρ represents the walk-off angle induced by the birefringence, L_0 is the common cavity optical path length, L_1 and L_2 are the respective optical thicknesses of the two crystals; ε is the additional optical path length difference introduced by wedges and/or tolerances in the crystal

Optics EXPRESS

thickness. We consider the case of nominally identical crystal thicknesses ($L_1 = L_2$), we define $L_{tot} = L_0 + L_1 \cdot (1+1/\cos\rho)$ and, considering $\varepsilon \ll L_{tot}$, we write:

$$\Delta f_{rep} \cong \frac{c}{2} \cdot \frac{\varepsilon}{L_{tot}^2}. \tag{5}$$

Combining now Eq. (3) with Eq. (5), we obtain:

$$\varepsilon < \frac{c}{4\Delta f_{opt}}. \tag{6}$$

This describes the maximum path length difference to avoid aliasing. In the dual-comb MIXSEL, we could tune to $\varepsilon \approx 1$ µm, which would theoretically allow large optical bandwidth without aliasing of several tens of THz.

In order exploit the broad laser spectrum without spectral filtering, we prevent aliasing effects by choosing Δf_{rep} with the insertion of two 0.5 mm thick wedged intracavity BCs oriented orthogonally with respect to each other as shown in Fig. 1(a). The optical path difference arises from the crystal wedges and can be finely tuned by crystal translation. In addition, the two BCs preserve a sufficient separation of the cavity spots on the MIXSEL chip. The selected Δf_{rep} of 51.9 kHz (Fig. 1(f)) corresponds to a cavity length difference for the cross-polarized OFCs of only ≈1 µm, which results in an aliasing-free comb largely separated from its high- frequency replica (Fig. 1(e)). The entire laser setup delivering the dual-comb signal is built in a closed box with a total volume occupancy of 23 × 32 × 11 cm^3 (Fig. 1(g)).

5. Fourier transform analysis

The spectroscopic signal is generated by overlapping both beams in the same polarization in a fiber coupled 50:50 beam splitter and recording their beat note with a photodiode. The time domain signal is detected on a balanced detector (Thorlabs PDB481C-AC) and recorded at a sampling rate of 2.5 GS/s on a digitizing oscilloscope (Teledyne LeCroy 6104) with 1 GHz bandwidth. The total measurement time of 100 ms is currently limited by internal memory of the oscilloscope but could easily be extended with suitable electronics. The recorded time-domain trace (Fig. 2(a)) consists of a sequence of interferograms (inset) repeating every 19 µs ($1/\Delta f_{rep}$).

The frequency domain spectrum is obtained with Fourier transform analysis. Parasitic intracavity reflection between the non-wedged surface of the BC and the OC produce secondary interferograms symmetrically spaced 3.3 µs from the main interferograms. These parasitic back reflections are replaced by the mean value of the interferogram. Next, the average half maximum signal-to-noise-ratio (SNR) in frequency is observed for various integration times. The SNR increases up to a value of 200 µs, the mutual coherence time of the two OFCs. For longer temporal segments, the comb lines blur out due to drifts in Δf_{CEO}. The time domain trace is then sliced to segments of 200 µs and a 6-fold zero filling is applied for interpolation in the frequency domain. Fast-Fourier-Transform is performed per segment without apodization and yields the complex Fourier domain signal *I'(f)* with a cardinal sinus instrumental response.

Measurement induced phase errors are corrected by standard means [28]: The phase of the spectrum $\angle\ \theta$ is calculated at the comb line positions from real and imaginary part of the complex Fourier transform $I'(f)$:

$$\arctan(\theta) = \frac{\mathrm{Im}(I'(f))}{\mathrm{Re}(I'(f))}. \tag{7}$$

Optics EXPRESS

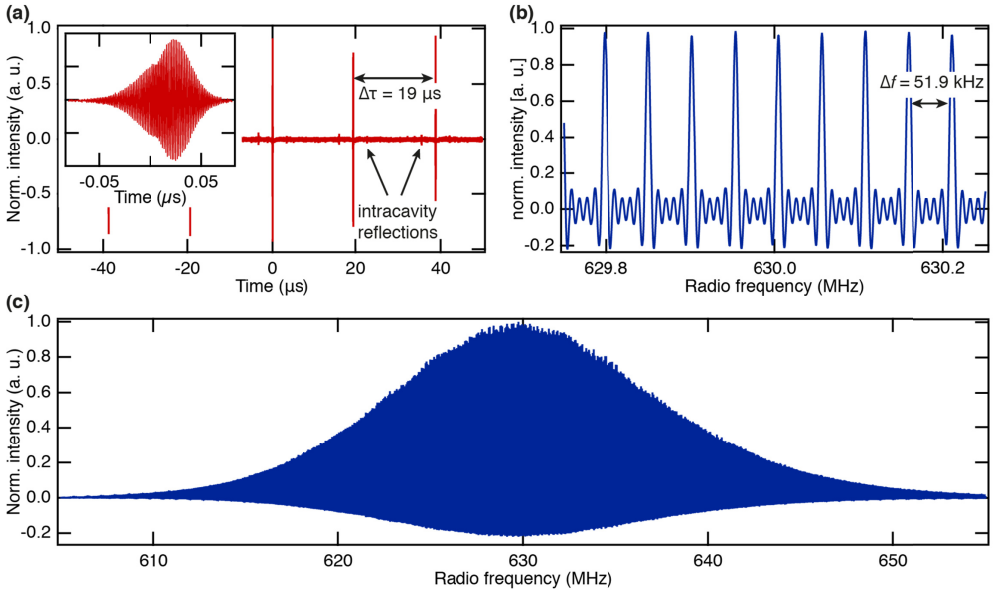

Fig. 2. Time and frequency domain dual-comb signal. a) Time domain dual-comb interferogram. The periodicity of the interference bursts reproduces the inverse of Δf_{rep}. Intracavity reflections generate smaller bursts ± 3.3 μs apart from the main peak, corresponding to the 9 mm distance BC-OC. Inset: expansion of an interference burst. The asymmetric interferogram is due to insufficient sampling (2.5 GS/s, with a pulse repetition frequency of 2.73 GHz). b) Expanded part of c: Comb teeth obtained through phase-corrected Fourier transform of 200-μs time segments. Therefore, the individual comb lines show the characteristic sinc instrumental line shape. c) Microwave spectrum of the 100 ms time trace. More than 1000 lines are simultaneously resolved.

The phase is then estimated at the intermediate points using a spline interpolation. The true spectrum is finally recovered using

$$I(f) = \mathrm{Re}\left(I'(f)\right)\cos(\theta) + \mathrm{Im}\left(I'(f)\right)\sin(\theta). \quad (8)$$

Drifts in Δf_{rep} change the span of the detected comb and manifest themselves in a change in line spacing of the detected comb, while drifts in Δf_{CEO} induce a translation of the radio frequency spectrum. Fluctuations of the line spacing are not observable over the measurement time duration of 100 ms and indicate a stable Δfrep. Drifts in Δf_{CEO} are observed by tracking the motion of individual comb lines between subsequent segments and remain below Δf_{rep} = 51 kHz over the measurement time of 100 ms The frequency scale of each spectrum is then translated, such that the comb lines from the different segments overlap before averaging in frequency domain.

The phase-corrected Fourier spectrum reveals the down-converted radio frequency comb centered at 630 MHz and spanning 50 MHz, consistently with the MSA measurement (Figs. 2(b) and 2(c)). The instrumental cardinal sine line-shape of an unapodized interferogram is visible in the clearly resolved 1067 teeth of the radio frequency comb. The number of comb lines is about one order of magnitude higher compared to other semiconductor dual-comb systems like QCLs [14,15] and ICLs [16,17].

We define the spectral noise as the standard deviation of the microwave spectrum taken in the 505-550 MHz region, at lower frequencies than those occupied by the comb envelope. We assume the noise to stay constant over the dual-comb spectral range. From the ratio between the half maximum of the spectra envelope of the dual-comb spectrum and the spectral noise, we obtain an SNR of ~70, which results in an SNR per unit of time of 230 $s^{-1/2}$. The figure of merit (FOM) of 2.5 × 10^5 $s^{-1/2}$ is obtained by multiplying the SNR per unit of time for the

Optics EXPRESS

number of resolved comb lines. The FOM can be improved with better VBG (volume Bragg grating)-stabilized pump diodes [29]. Additionally, SNR could be significantly improved by an engineered prototype housing with minimized mechanical vibrations and air turbulences.

6. Dual-comb spectroscopy

Finally, we perform free-running dual-comb spectroscopy (DCS) by directing one OFC through a commercial multi-mode-fiber-coupled, multipass cell with a total absorption length of 80 cm containing acetylene (C_2H_2) at room temperature with a nominal pressure of 987 Pa ± 10% (Fig. 3(a)). At this pressure, the absorption lines of acetylene are broadened to more than 6 GHz and can be sampled with the line spacing of 2.73 GHz. The absorption in the gas cell is governed by Beer-Lambert-Law:

$$I(f) = I_0(f)e^{-\alpha(f)nl}. \tag{9}$$

This formula describes the transmission of light through a gas cell of length l, where $I_0(f)$ is the incident light intensity and $I(f)$ is the transmitted intensity as function of frequency (red in Fig. 3(b)). The number density $n = N/V$ can be related to the pressure p via temperature T, volume V and the Boltzmann konstant k_B using the ideal gas law:

$$n = \frac{N}{V} = \frac{p}{k_B T}. \tag{10}$$

The absorption cross-section $\alpha(f)$ governs the frequency-dependent absorption. With the absorption cross-section being a summation of Lorentzian peaks $P_i(f)$:

$$\alpha(f) = \sum_i P_i(f). \tag{11}$$

Herewith the absorption results in a multiplicative law as follows:

$$I(f) = I_0(f) \cdot \prod_i e^{-\frac{pl}{k_B T} P_i(f)}. \tag{12}$$

The lines $R(12)$ to $R(26)$ of the $3\nu_3$ band of $^{12}C_2H_2$, coincide with the last ≈0.8 THz of the low-frequency tail of the MIXSEL optical spectrum (Fig. 3(b)). We calibrate our retrieved spectrum against a spectrum computed using the parameters from the HITRAN 2016 database for an *a posteriori* calibration of the frequency scale [30]. To extract the transmittance of the sample, we use a logarithmic version of Eq. (12):

$$-\ln\left(I(f)\right) = -\ln\left(I_0(f)\right) + \frac{pl}{k_B T} \sum_i P_i(f). \tag{13}$$

where $-\ln(I_0(f))$ represents the baseline fit of the comb envelope. Data and fit are then divided by the baseline, according to Eq. (12), to yield the transmittance (Figs. 3(c) and (d)).

Without active stabilization and locking electronics, the overlay of the experimentally acquired dual-comb transmission follows line-by-line the characteristic acetylene transmission envelope as computed from the HITRAN 2016 database (Figs. 3(c) and 3(d)). The residuals and the standard deviation of 0.028 attests good transmission intensity precision to our dual-comb spectrometer.

Optics EXPRESS

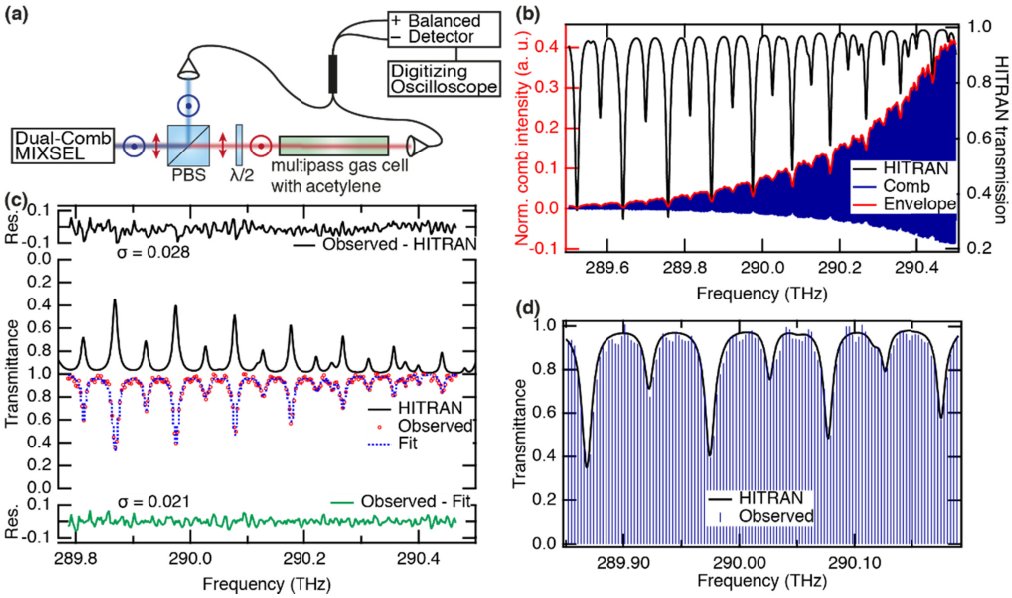

Fig. 3. Dual-Comb spectroscopy of acetylene with a free-running dual-comb MIXSEL. a) Schematic of the DCS experimental setup. One pulse train interrogates the absorption of the sample in the multipass cell and is combined with the second comb in a fiber BS, whose two outputs are balance-detected. b) DCS spectrum recalibrated in the optical domain. The absorption lines visible in the comb envelope are matched with the HITRAN database to provide frequency calibration. c) Transmission spectrum of the *R*-branch of the $3\nu_3$ band of acetylene acquired with the unstabilized dual-comb MIXSEL spectrometer. The spectral envelope of the comb is fitted by the product of a baseline and Lorentzian line profiles. The residuals between the observed points and the HITRAN database are plotted in black, the one between observed points and fit in green. d) Portion of the transmission spectrum compared with the HITRAN database.

7. Conclusion and outlook

With this new technology, we can profit from the high peak power of the modelocked pulses and passively broaden the MIXSEL spectrum in silicon nitride waveguides [29] and generate broadband mid-infrared (mid-IR) combs [31] for extended spectroscopic potential. Coherent anti-Stokes Raman spectroscopy (CARS) [32] as well as light detection and ranging (LIDAR) are applications that could benefit from the fast and manageable dual-comb MIXSEL in the near future.

In future steps, we will extend the intrinsic simplicity of the MIXSEL dual-comb spectrometer to other wavelength regions. The chip used in this work emits in the near-IR range although most of the relevant molecular fingerprints for industrial and environmental applications lie in the mid-IR spectral domain. To date semiconductor bandgap engineering has enabled optically pumped semiconductor disk lasers from the UV to the mid-IR [18]. Optically pumped GaSb-based semiconductor disk lasers have been successfully demonstrated in the 2-3 µm wavelength range [33] and first successful modelocking with 384 fs pulses has been demonstrated at 2 µm [34]. Our next focus is to extend the near-IR MIXSELs to the mid-IR additionally using type-II InAs-GaSb-based quantum wells [ERC Advanced Grant 787079 ONE-MIX (2018)].

Funding

ETH Research (ETH-49 18-1).

Optics EXPRESS

Acknowledgments

This work was supported by ETH Research and the technology and cleanroom facility FIRST of ETH Zurich for advanced micro- and nanotechnology.

References

1. H. R. Telle, G. Steinmeyer, A. E. Dunlop, J. Stenger, D. H. Sutter, and U. Keller, "Carrier-envelope offset phase control: A novel concept for absolute optical frequency measurement and ultrashort pulse generation," Appl. Phys. B **69**(4), 327–332 (1999).
2. D. J. Jones, S. A. Diddams, J. K. Ranka, A. Stentz, R. S. Windeler, J. L. Hall, and S. T. Cundiff, "Carrier-envelope phase control of femtosecond mode-locked lasers and direct optical frequency synthesis," Science **288**(5466), 635–640 (2000).
3. A. Apolonski, A. Poppe, G. Tempea, C. Spielmann, T. Udem, R. Holzwarth, T. W. Hänsch, and F. Krausz, "Controlling the phase evolution of few-cycle light pulses," Phys. Rev. Lett. **85**(4), 740–743 (2000).
4. J. Reichert, R. Holzwarth, T. Udem, and T. W. Hänsch, "Measuring the frequency of light with mode-locked lasers," Opt. Commun. **172**(1-6), 59–68 (1999).
5. I. Coddington, N. Newbury, and W. Swann, "Dual-comb spectroscopy," Optica **3**(4), 414–426 (2016).
6. S. Coburn, C. B. Alden, R. Wright, K. Cossel, E. Baumann, G.-W. Truong, F. Giorgetta, C. Sweeney, N. R. Newbury, K. Prasad, I. Coddington, and G. B. Rieker, "Regional trace-gas source attribution using a field-deployed dual frequency comb spectrometer," Optica **5**(4), 320–327 (2018).
7. Z. Chen, M. Yan, T. W. Hänsch, and N. Picqué, "A phase-stable dual-comb interferometer," Nat. Commun. **9**(1), 3035 (2018).
8. G. Ycas, F. R. Giorgetta, E. Baumann, I. Coddington, D. Herman, S. A. Diddams, and N. R. Newbury, "High-coherence mid-infrared dual-comb spectroscopy spanning 2.6 to 5.2 μm," Nat. Photonics **12**(4), 202–208 (2018).
9. T. Ideguchi, T. Nakamura, Y. Kobayashi, and K. Goda, "Kerr-lens mode-locked bidirectional dual-comb ring laser for broadband dual-comb spectroscopy," Optica **3**(7), 748–753 (2016).
10. X. Zhao, G. Hu, B. Zhao, C. Li, Y. Pan, Y. Liu, T. Yasui, and Z. Zheng, "Picometer-resolution dual-comb spectroscopy with a free-running fiber laser," Opt. Express **24**(19), 21833–21845 (2016).
11. R. Liao, Y. Song, W. Liu, H. Shi, L. Chai, and M. Hu, "Dual-comb spectroscopy with a single free-running thulium-doped fiber laser," Opt. Express **26**(8), 11046–11054 (2018).
12. G. Millot, S. Pitois, M. Yan, T. Hovhannisyan, A. Bendahmane, T. W. Hänsch, and N. Picqué, "Frequency-agile dual-comb spectroscopy," Nat. Photonics **10**(1), 27–30 (2016).
13. M.-G. Suh, Q.-F. Yang, K. Y. Yang, X. Yi, and K. J. Vahala, "Microresonator soliton dual-comb spectroscopy," Science **354**(6312), 600–603 (2016).
14. G. Villares, A. Hugi, S. Blaser, and J. Faist, "Dual-comb spectroscopy based on quantum-cascade-laser frequency combs," Nat. Commun. **5**(1), 5192 (2014).
15. Q. Y. Lu, S. Manna, D. H. Wu, S. Slivken, and M. Razeghi, "Shortwave quantum cascade laser frequency comb for multi-heterodyne spectroscopy," Appl. Phys. Lett. **112**(14), 141104 (2018).
16. M. Bagheri, C. Frez, L. A. Sterczewski, I. Gruidin, M. Fradet, I. Vurgaftman, C. L. Canedy, W. W. Bewley, C. D. Merritt, C. S. Kim, M. Kim, and J. R. Meyer, "Passively mode-locked interband cascade optical frequency combs," Sci. Rep. **8**(1), 3322 (2018).
17. L. A. Sterczewski, J. Westberg, C. L. Patrick, C. S. Kim, M. Kim, C. L. Canedy, W. W. Bewley, C. D. Merritt, I. Vurgaftman, J. R. Meyer, and G. Wysocki, "Multiheterodyne spectroscopy using interband cascade lasers," Opt. Eng. **57**, 011014 (2017).
18. M. Guina, A. Rantamäki, and A. Härkönen, "Optically pumped VECSELs: review of technology and progress," J. Phys. D Appl. Phys. **50**(38), 383001 (2017).
19. B. W. Tilma, M. Mangold, C. A. Zaugg, S. M. Link, D. Waldburger, A. Klenner, A. S. Mayer, E. Gini, M. Golling, and U. Keller, "Recent advances in ultrafast semiconductor disk lasers," Light Sci. Appl. **4**, e310 (2015).
20. S. M. Link, D. J. H. C. Maas, D. Waldburger, and U. Keller, "Dual-comb spectroscopy of water vapor with a free-running semiconductor disk laser," Science **356**(6343), 1164–1168 (2017).
21. J. Davila-Rodriguez, M. Bagnell, C. Williams, and P. J. Delfyett, "Multiheterodyne Detection for Spectral Compression and Downconversion of Arbitrary Periodic Optical Signals," J. Lightwave Technol. **29**(20), 3091–3098 (2011).
22. D. J. H. C. Maas, A.-R. Bellancourt, B. Rudin, M. Golling, H. J. Unold, T. Südmeyer, and U. Keller, "Vertical integration of ultrafast semiconductor lasers," Appl. Phys. B **88**(4), 493–497 (2007).
23. S. M. Link, A. Klenner, M. Mangold, C. A. Zaugg, M. Golling, B. W. Tilma, and U. Keller, "Dual-comb modelocked laser," Opt. Express **23**(5), 5521–5531 (2015).
24. M. Mangold, C. A. Zaugg, S. M. Link, M. Golling, B. W. Tilma, and U. Keller, "Pulse repetition rate scaling from 5 to 100 GHz with a high-power semiconductor disk laser," Opt. Express **22**(5), 6099–6107 (2014).
25. C. G. E. Alfieri, D. Waldburger, J. Nürnberg, M. Golling, and U. Keller, "Sub-150-fs pulses from an optically pumped broadband modelocked integrated external-cavity surface emitting laser," Opt. Lett. **44**(1), 25–28 (2019).

Optics EXPRESS

26. O. D. Sieber, M. Hoffmann, V. J. Wittwer, M. Mangold, M. Golling, B. W. Tilma, T. Südmeyer, and U. Keller, "Experimentally verified pulse formation model for high-power femtosecond VECSELs," Appl. Phys. B **113**(1), 133–145 (2013).
27. C. E. Shannon, "Communication in the presence of noise," reprint in Proc. IEEE **86**(2), 447–457 (1998).
28. P. R. Griffith and J. A. de Haseth, Fourier Transform Infrared Spectrometry (John Wiley & Sons, Hoboken, New Jersey, 2007).
29. A. Klenner, A. S. Mayer, A. R. Johnson, K. Luke, M. R. E. Lamont, Y. Okawachi, M. Lipson, A. L. Gaeta, and U. Keller, "Gigahertz frequency comb offset stabilization based on supercontinuum generation in silicon nitride waveguides," Opt. Express **24**(10), 11043–11053 (2016).
30. I. E. Gordon, L. S. Rothman, C. Hill, R. V. Kochanov, Y. Tan, P. F. Bernath, M. Birk, V. Boudon, A. Campargue, K. V. Chance, B. J. Drouin, J. M. Flaud, R. R. Gamache, J. T. Hodges, D. Jacquemart, V. I. Perevalov, A. Perrin, K. P. Shine, M. A. H. Smith, J. Tennyson, G. C. Toon, H. Tran, V. G. Tyuterev, A. Barbe, A. G. Császár, V. M. Devi, T. Furtenbacher, J. J. Harrison, J. M. Hartmann, A. Jolly, T. J. Johnson, T. Karman, I. Kleiner, A. A. Kyuberis, J. Loos, O. M. Lyulin, S. T. Massie, S. N. Mikhailenko, N. Moazzen-Ahmadi, H. S. P. Müller, O. V. Naumenko, A. V. Nikitin, O. L. Polyansky, M. Rey, M. Rotger, S. W. Sharpe, K. Sung, E. Starikova, S. A. Tashkun, J. V. Auwera, G. Wagner, J. Wilzewski, P. Wcisło, S. Yu, and E. J. Zak, "The HITRAN2016 molecular spectroscopic database," J. Quant. Spectrosc. Radiat. Transf. **203**, 3–69 (2017).
31. A. S. Mayer, C. R. Phillips, C. Langrock, A. Klenner, A. R. Johnson, K. Luke, Y. Okawachi, M. Lipson, A. L. Gaeta, M. M. Fejer, and U. Keller, "Offset-Free Gigahertz Midinfrared Frequency Comb Based on Optical Parametric Amplification in a Periodically Poled Lithium Niobate Waveguide," Phys. Rev. Appl. **6**(5), 054009 (2016).
32. T. Ideguchi, S. Holzner, B. Bernhardt, G. Guelachvili, N. Picqué, and T. W. Hänsch, "Coherent Raman spectro-imaging with laser frequency combs," Nature **502**(7471), 355–358 (2013).
33. P. Holl, M. Rattunde, S. Adler, S. Kaspar, W. Bronner, A. Bächle, R. Aidam, and J. Wagner, "Recent Advances in Power Scaling of GaSb-Based Semiconductor Disk Lasers," IEEE J. Sel. Top. Quantum Electron. **21**(6), 324–335 (2015).
34. A. Harkönen, C. Grebing, J. Paajaste, R. Koskinen, J. P. Alanko, S. Suomalainen, G. Steinmeyer, and M. Guina, "Modelocked GaSb disk laser producing 384 fs pulses at 2 µm wavelength," Electron. Lett. **47**(7), 454–456 (2011).